Advanced Retrievals of Multilayered Cloud Properties Using Multi-Sensor and Multi-Spectral Measurements

Jianping Huang
Analytical Services & Materials, Inc
Hampton, VA

Patrick Minnis, Bing Lin
NASA Langley Research Center
Hampton VA

Yuhong Yi, Mandana M. Khaiyer
Analytical Services & Materials, Inc.
Hampton, VA

Robert F. Arduini, Alice Fan
SAIC, Hampton, VA

Gerald G. Mace
Dept. of Meteorology, University of Utah
Salt Lake City, Utah

Abstract

Current satellite cloud retrievals are usually based on the assumption that all clouds consist of a homogenous single layer, despite the frequent occurrence of cloud overlap. As such, cloud overlap will cause large errors in the retrievals of many cloud properties. To address this problem, a multilayered cloud retrieval system (MCRS) is developed by combining satellite visible and infrared radiances and surface microwave radiometer measurements. A two-layer cloud model was used to simulate multilayered cloud radiative characteristics and to parameterize the total-column visible reflectance. The radiances emanating from the combined low cloud and surface are estimated using the microwave liquid water with an assumption of effective droplet size. These radiances replace the radiances traditionally used in single-layer cloud retrievals. The MCRS was applied to 8 months data from March to October, 2000 over four Atmospheric Radiation Measurement (ARM) Southern Great Plains (SGP) sites. The results were compared to the available retrievals of ice water path (*IWP*) from radar data and show that the MCRS clearly produces a more accurate retrieval of multilayered cloud properties. MCRS yields values of *IWP* that are closest to those from the radar retrieval. For ice-over-water cloud systems, on average, the optical depth and *IWP* were reduced, from original overestimates, by approximately 30.0%. The March-October mean temperatures from the MCRS were decreased by 10 $\pm$ 12 K, which translates to a height difference of ~1.4 km. These results indicate that ice-cloud height derived from traditional single-layer retrieval is underestimated and the mid-level ice cloud coverage is over classified. Effective ice crystal particle sizes are increased by only a few percent with the new method. Sensitivity tests suggest that this method is not particularly sensitive to the assumed water droplet size and the uncertainties in the microwave retrievals. This new physically based technique should be robust

and directly applicable when satellite imager and the proper satellite or surface microwave data are available.

Key Word: Cloud Retrieval, Multilayer, Overlap, Microwave, Ice cloud, Ice water path

1. Introduction

Clouds, especially high clouds, are very important regulators of the hydrological and energy cycle of Earth's climate. Although the critical role of clouds in Earth's radiation balance has been widely recognized for many years, they are still the major source of large uncertainties in climate predictions by general circulation models (GCMs). The difficulty in adequately capturing the cloud radiative effects in GCMs is well documented [*Cess et al.* 1990]. One of the principal reasons for the large uncertainties is the poor knowledge of ice water path (*IWP*) distribution. Until the *IWP* is properly characterized by observations, it will not be possible to sufficiently constrain, for the sake of reliable climate assessment, the models' production of ice water and its subsequent effects on the hydrological and radiation budgets. Thus, globally accurate *IWP* information is urgently needed for testing of global climate models and characterizing the radiation budget.

IWP determination is often complicated because of cloud overlap. Current satellite *IWP* retrievals are usually based on the assumption that all clouds are single-layered, despite the relatively frequent occurrence of overlapped cloud systems. Cloud overlap can cause large errors in the retrievals of many properties including cloud height, optical depth, thermodynamic phase, and particle size. For multilayered clouds, one of the greatest impediments to accurately determine cloud ice mass for a given atmospheric profile is the influence of underlying liquid water clouds and precipitation on the radiances observed at the top-of-atmosphere (TOA) in the visible and near-infrared wavelengths. Although *IWP* can be inferred from retrievals of cloud optical depth and effective ice particle sizes using visible (VIS) and infrared (IR) methods [e.g., *Minnis et al.* 1993, 1995, 1998, 2001], it is generally overestimated when water clouds are present underneath the ice clouds. The optical depth derived from the reflected

VIS-IR radiances represents the combined effects of all cloud layers and the resulting *IWP* is actually an estimate of the total water path (*TWP*). When the multilayered cloud is retrieved as if it were an ice cloud, the larger sizes of the ice crystals tend to yield a greater IWP (*TWP*) than would be expected from the simple summation of the actual *IWP* and *LWP* in the column. Thus, the effects of the *LWP* and *IWP* in multilayered cloud systems should be separated.

Methods for direct retrievals of ice cloud properties using millimeter and sub-millimeter-wavelength measurements in all conditions [*Liu and Curry* 1998, 1999; *Weng and Grody* 2000; *Zhao and Weng* 2002] are under development but have not yet been deployed on satellites. However, even for these newer techniques there are no cloud property estimates for the lower cloud layers in multi-layer systems.

Currently, the most feasible approach for retrieving *IWP* for the overlapped cases uses a combination of microwave (MW) and VIS-IR methods. Although the VIS-IR retrievals of optical depths and effective particle sizes are for the whole column of clouds, in multilayered clouds, they are primarily sensitive to the upper cloud layer, especially when the upper-layer ice clouds are thick. Microwave radiation, on the other hand, is mainly affected by surface, water clouds and atmospheric water vapor; it is not significantly scattered or absorbed by ice clouds. Therefore, over oceans, which have a predictable surface emissivity, it is possible to combine both VIS-IR and MW techniques to determine the presence of water clouds below the ice clouds and separately estimate *IWP* and *LWP* for each scene. *Lin and Rossow* [1996] estimated global *IWP* distributions over oceans by using a simple separation technique of total water path (*TWP*), which is assumed to be equal to the combination of *LWP* and *IWP*, retrieved from VIS/IR data by the International Satellite Cloud and Climatology Project (ISCCP) and cloud liquid water path (*LWP*) from a MW remote sensing method, respectively. In that

case, the ISSCP and MW data were matched only 1.5 hr on temporal resolution and 30KM on spatial resolution. A more refined MW, VIS, and IR (MVI) technique [*Lin et al.* 1998] was used to derive *IWP* in the same manner using well-matched instantaneous Visible Infrared Scanner (VIRS) and Tropical Rainfall Measuring Mission (TRMM) Microwave Imager (TMI) data taken by *TRMM* over ocean [*Ho et al.* 2003]. Those estimates mark an advance in our knowledge of global *IWP* but they are limited to ocean areas, are based on the simple TWP-*LWP* difference technique, and are difficult to validate.

Over land, the variability in surface emissivity renders such an approach nearly useless. However, at several Atmospheric Radiation Measurement (ARM) Program [*Ackerman and Stokes*, 2003] surface sites, *LWP* is routinely derived from MW radiometers and, at one location, cloud vertical structure is determined accurately from a combination of cloud lidars and radars. In some cases, it is possible to simultaneously derive the *IWP* from the radar data even when *LWP* is present [*Mace et al.* 2002]. Cloud properties have been derived every half hour for several years from VIS-IR imager data taken by the Geostationary Operational Environmental Satellites (*GOES*) using the Visible Infrared Solar-infrared Split-window Technique (VISST; see *Minnis et al.* [2002]). Initial comparisons of the *IWP* retrieved from *Terra* Moderate Resolution Imaging Spectroradiometer data with ARM radar retrievals [*Mace et al.* 2004] indicate that for cirrus clouds with *IWP* as large as 120 gm^{-2}, the mean *IWP* from VISST is within 5% of the radar retrieval. Instantaneous VISST retrievals are within 25% of the radar results. Those initial comparisons indicate that the satellite and radar methods yield similar results for single-layered ice clouds. By combining the *GOES* satellite retrievals with the surface-derived *LWP* over the ARM sites, it should be possible to develop a more complete *IWP* climatology over this limited region for single- and multilayered clouds and perform some validation comparisons with the

surface-based *IWP* retrievals for multilayered clouds.

In this paper, an improved technique is developed to estimate *LWP* and *IWP* values simultaneously using satellite and ground-based measurements over ARM Southern Great Plains (SGP) boundary and central facilities sites. Rather than simply differencing the TWP and MW *LWP* in overlapped cases, this new approach performs a more explicit radiance-based retrieval of IWP to account for differences in the optical properties of ice and liquid water clouds. In overlapped cases, *LWP* is estimated from ARM MW radiometer (MWR) measurements first, and then used as lower boundary for a reanalysis of the satellite *IWP* retrieval. In the initial VISST analysis for overlapped clouds, *IWP* is derived assuming the entire cloud is composed of ice crystals; the surface and atmosphere together form the lower boundary condition for the retrieval. The new algorithm will treat the combination of the lower cloud, the atmosphere, and the surface as the lower boundary condition. The *IWP* retrievals are then based on the calculation of the integrated systems of upper level ice clouds and the lower boundaries using a radiative transfer model parameterization. Preliminary validation of the retrievals is accomplished by comparisons with simultaneous retrievals using the ARM radar at the SGP Central Facility (SCF).

2. Satellite and Surface Data

2.1 VISST

This study analyzes satellite and surface measurements taken between 1 March and 30 October 2000 over the ARM SGP domain. GOES-8 provided continuous coverage of the region and was used to derive the daytime cloud properties using the VISST, which is an upgrade of the 3-channel method

described by *Minnis et al.* [1995]. VISST analyzes an array of satellite-observed VIS (0.65 μm) reflectances and 3.9, 10.8, and 12.0 μm brightness temperatures at a given set of solar zenith, viewing zenith, and relative azimuth angles using a set of lookup tables in parameterizations [*Minnis et al.*, 1998] that account for the contributions of the surface and atmosphere to the radiance in each channel. Solutions are computed iteratively for both liquid and ice clouds yielding effective droplet size r_e or effective ice crystal diameter *De*, optical depth t, and cloud radiating temperature *Tc*. Phase is determined using several criteria including the value of *Tc*, the available solution, and the consistency of the temperature parameterized using the retrieval with the observed value. *IWP* or *LWP* is computed from the particle size and optical depth. The GOES-8 VIS radiances were calibrated against VIRS as described by *Minnis et al.* [2002].

2.2 Microwave retrievals

An algorithm adapted from the satellite remote sensing method of *Lin et al*. [1998, 2001] was used to retrieve *LWP* and liquid water temperature *Tw* from the ground-based ARM SGP MW radiometer (MWR) and infrared thermometer (IRT) measurements. ARM's ground-based MWRs are available at several locations within the SGP domain: site B1 located at 38.31°N, 97.30°W (Hillsboro, OK); B4 at 36.07°N, 99.20°W (Vici, OK); B5 at 35.69°N, 95.87°W (Morris, OK); and the SCF C1 at 36.61°N, 97.49°W (Lamont, OK). Cloud base height information was determined using Vaisala ceilometer data at sites B1, B4 and B5 and ARSCL (Active Remote Sensing of Cloud Layers; see *Liljegren* [1999]; *Clothiaux et al.* [2000]) data at C1 (the SCF). Surface pressure and air temperature, as well as temperature and wind direction at cloud base height, were provided by Rapid Update Cycle (RUC; see *Benjamin et al.* [2004]) 3-hourly model output. The ARM MWRs measure 23.8 and 31.4 GHz brightness temperatures at 20-second sampling intervals. Before retrieving *LWP*

and *Tw*, the 2-s data were averaged over 3-minute intervals to reduce *Tb* measurement noise and facilitate processing.

2.3 MVI overlapped cloud selection

The GOES-8 radiances and cloud properties were averaged in 0.3° boxes centered on each site and matched with half-hourly averaged MWR-retrieved cloud properties. Overcast clouds constitute about 74.2% of all of the cloudy cases. The overcast cases can be further classified as 18% ice, 38% liquid water, and 18% mixed phase. Since the IRT provides only one temperature for the site and no information about partial cloudiness, no broken clouds are considered further here. To take into account the advantages of each technique, only those clouds classified as overcast ice-phase clouds by VISST are examined.

The overcast ice phase clouds actually consist of single-layered ice clouds and ice-over-water cloud. The ice-over-water clouds are identified using the MVI method, which uses the difference between cloud liquid water temperature *Tw* and the effective cloud temperature *Tc*. The cloud liquid water temperature *Tw* retrieved from IRT data is close to cloud base temperature, especially when the lower level clouds are thick [*Lin et al.* 2001] whereas the effective cloud temperature *Tc* derived from GOES data represents the temperature near the top of the cloud for optically thick clouds [*Minnis et al.* 1993]. When the difference, $DTwc = Tw - Tc$, is significantly larger than zero, it is likely that the observed system consists of overlapped or mixed phase clouds [*Lin et al.* 1998; *Ho et al.* 2003]. In this study, the conditions required for classifying a cloud as ice-over-water for the entire 0.3° box is: 100% ice phase, $Tc < 273$K, $Tw\text{-}Tc > 8$ K and MWR *LWP* (LWP_{MW}) > 0.0 gm^{-2}. Multilayered clouds were detected in 60% of the total occurrences of overcast ice clouds from all four sites. Most of

the overlapped cloud systems consist of cold, high ice cloud over lower, warmer water cloud [*Huang et al.*, 2003].

3. Development of Multilayered Cloud Retrieval System (MCRS)

In the MVI method, it is assumed that, for overcast multilayered ice-over-water clouds, the VISST-derived *IWP* equals *TWP*. Therefore, the "true" ice water is estimated by the MVI technique through simple differencing as

$$IWP = TWP - LWP, \quad (1)$$

where *LWP* is from the MWR retrieval. In reality, the microphysical properties of the low-level clouds significantly influence the VISST-derived optical depths and effective diameters subjecting the simple differencing method to potentially large biases. To illustrate this point, adding-doubling radiative transfer calculations of VIS reflectance were performed using the microphysical model (T40; *De* = 67.6 μm; see *Minnis et al.* [1998]) for an ice cloud at a temperature of -40°C for various optical depths as a single-layered cloud and as part of a two-layered cloud system. In the latter case, the lower layer was assumed to be a water cloud with effective droplet radii, *re* = 8 μm (r8) and 12 μm (r12), and *LWP* = 100 gm^{-2}. The VIS reflectance was computed for both the single and multilayered clouds for *TWP* up to 600 gm^{-2}. Examples of the results are plotted in Figure 1 for two solar zenith q_o, one viewing zenith q (45°), and three relative azimuth f angles. In the top panel, the reflectance (thin curve) for q_o = 60°, f = 25° and T40 increases from 0.52 at *TWP* = 100 gm^{-2} to 0.66 for *TWP* = 200 gm^{-2} up to 0.84 for *TWP* = 600 gm^{-2}. The reflectance (thick curve) for T40 at q_o = 30° starts at a lower value and follows a

similar curve. If lower-level clouds exist, the reflectances are higher than those of single layer clouds for a given *TWP*. For example, for *TWP* around 100 gm^{-2} (*LWP* = 100 gm^{-2}, *IWP* ~ 0), T40/r12, and q_o = 60°, the reflectance is 0.65, while the single-layer ice clouds with the same amount of *TWP* would produce 0.52 reflection. This effect causes current satellite retrievals to overestimate *IWP* or TWP when the lower cloud is present. An assumed cloud with both *IWP* and *LWP* equal to 100 gm^{-2} (*TWP* = 200 gm^{-2}) would have a reflectance 0.73. The current VISST retrieval would assume that the entire cloud is in ice phase, and then, following the T40 curve, obtain *IWP* = *TWP* = 300 gm^{-2}. If a MW retrieval of *LWP* = 100 gm^{-2} is used to estimate *IWP*, the MVI method would yield 200 gm^{-2} instead of 100 gm^{-2}. The error is even worse for the T40/r8. While the forward scattering direction (f = 25°) represents an extreme case, most of the other results (seen in the lower panels of Figure 1) would yield overestimates of *IWP* using the MVI approach. Since the operational VISST uses *t* and *De* as its retrieval products, and water cloud droplets are much smaller (a factor of 2~3) than ice crystals, most of the overestimation discussed above is compensated through underestimation of column total optical depths and overestimation of averaged column effective particle sizes. Nevertheless, there are significant errors inherent in the MVI algorithm that will depend on the viewing and illumination angles and relative amounts of ice and water.

To improve the accuracy of ice cloud property retrievals, a new retrieval algorithm is developed for multilayered cloud system. A schematic view of this new algorithm, the multilayered cloud retrieval system (MCRS), is outlined in Figure 2. Initially, the VISST retrieval is performed using the surface as the background and the MWR retrieval is used to derive *LWP* and *Tw*. The results are used in the MVI method to detect the cloud overlapping by using the difference between the value of cloud water temperature *Tw* retrieved from IRT data and the cloud effective temperature *Tc* derived from satellites.

When the difference, *?Twc = Tw - Tc*, is significantly positive, it is likely that the observed system consists of overlapped clouds [*Lin et al.* 1998b; *Ho et al.* 2003; *Huang et al.* 2003]. Second, the optical depth of the low-level water cloud is estimated as

$$\tau_{low} = 0.75\, Q_{vis}(r_e)\, LWP_{MW} / r_e. \quad (2)$$

where $Q_{vis}(r_e)$ is the extinction efficiency at a given effective droplet radius. In this study, r_e is assumed to be 8 μm. The value of LWP_{MW} is from the MWR retrieval. In the third step, the combined reflectance is calculated by first computing the direct and diffuse reflectance at 0.65 for the combined surface, low water cloud, and atmosphere below the low water cloud to serve as the background reflectance field for a second VISST retrieval. Similarly, the value of *Tw* is adjusted to replace the surface skin temperature used in the initial retrieval and serves to provide the background emitted radiances at 3.9, 10.8, and 12.0 μm. Since the cloud water temperature derived from the MWR is close the cloud bottom temperature, the water cloud top temperature is given by

$$T_{wc} = T_w - gDZ/R \quad (3)$$

where *g* and *R* are the constant; *DZ* is water cloud thickness which is decided by (Minnis, et. al, 1995)

$$\Delta Z = 0.085\tau_{low}^{1/2}$$

The resulting VISST retrieval, therefore, accounts for the changes in the reflectance field due to the upper-layer cloud only. The low cloud-surface-lower atmosphere reflectance field is computed using the lookup tables of *Minnis et al.* [1998] in the parameterization reported by *Arduini et al.* [2002]. The new ice cloud-top temperature T_c is computed using the cloud emissivity. For optically thin water clouds, the ice cloud top temperature is estimated from the observed radiance:

$$B(T) = (1-\varepsilon_c)(1-\varepsilon_w)\,\varepsilon_s\,B(T_s) + (1-\varepsilon_c)\varepsilon_w B(T_{wc}) + \varepsilon_c B(T_c) \quad (4)$$

where ε_s ,e_c and e_w are the surface, upper layer ice cloud and lower-layer water cloud emissivities at 10.8 μm, respectively, and *B* is the Plank function evaluated at 10.8 μm. The values of e_c and ε_w are estimated as

$$\varepsilon_c = 1 - \exp[a(\tau_c/\mu)^b] \quad (5a)$$

and

$$\varepsilon_w = 1 - \exp[a(\tau_{low}/\mu)^b], \quad (5b)$$

respectively. The coefficients *a* and *b* depend on cloud microphysics (see *Minnis et al.* [1993]). Ts is surface skin temperature. When t_{low} is large (i.e, $\varepsilon_w = 1$), Equ.(4) can be simplified as

$$B(T) = (1-\varepsilon_c)B(T_{wc}) + \varepsilon_c B(T_c) \quad (6)$$

The new ice cloud properties, such as Tc, *t* and *De* from the second VISST retrieval are then used to calculate a new value of *IWP*. The only assumed microphysical parameter then is the effective droplet radius of the low-level cloud.

4. Case Studies

The application of the MCRS and the resulting changes in the ice cloud properties are best illustrated using a combination of surface-based passive and active sensors at the SCF. Figure 3 shows examples of cloud radar reflectivity signals of multilayered clouds over the SCF during 3 different days in 2000. The radar signals were obtained from the Millimeter Wave Cloud Radar (MMCR) system located at the SCF. The zenith-pointing MMCR system operates at 35 GHz and can probe the extent and composition of most clouds. These times were selected because the multi-layering conditions met the criteria for retrieving the ice cloud properties using the method of *Mace et al.* [2002]. As indicated in Table 1, these cases cover a wide range of viewing, illumination, and scattering angles. The value of q is constant at 47.64°. For this initial VISST retrieval, the value of *TWP* is equal to the *IWP*. As shown in Figure 3, the vertical structure of the multilayered cloud is complex. For example, in Figure 3d, a high (~10.5 km), cold (232.0 K) and thick ice cloud overlaps a low (~3 km), warm (284.8 K) and thin water cloud. The initial value of *Tc* from the VISST is about 53°C less than *Tw*, which translates to a height difference of ~7.5 km. The ice cloud thins out and splits in Figures 3e-f while the water layer thickens and is joined by another one. In Figure 3f, the ice cloud effective height and temperature from VISST are ~7.5 km and 255 K, respectively, and the MWR cloud water temperature is 287K. The retrieved ice cloud height is clearly less than the real upper layer cirrus altitude. The *LWP* is ~ 61 gm^{-2}, which is almost double the value in Figure 3d. Figures 3g-h also represent thick ice-over-water cloud cases except the lower layers are generally thicker than that in Figure 3c. A more complex case is seen in Figure 3a, where the lower level clouds may be doubled layered with a broken layer at bottom. Simpler cases are seen in Figures 3b, j, and k.

Table 1. Viewing, illumination, and scattering angles for GOES-8 and the surface at the SCF during 2000.

Case	Month	Date	Time (UTC)	q_o (°)	ϕ (°)	Scattering Angle (°)
1	March	22	1445	64.21	144.53	146.92
2	March	22	1515	58.66	150.27	154.21
3	March	22	1545	53.38	156.70	161.34
4	June	27	1745	16.88	173.54	148.00
5	June	27	1945	20.43	90.92	128.56
6	June	27	2015	25.65	79.37	122.37
7	June	27	2045	31.31	71.10	115.98
8	June	27	2152	37.18	64.67	109.41
9	July	3	1545	38.84	133.38	146.92
10	July	3	1615	32.95	139.53	149.88

Figure 4 compares the estimates of t, *De*, and *Tc* derived from the MCRS with those from the initial VISST for the cases in Figure 3. For all cases, the MCRS reduced the originally overestimated ice cloud optical depth (Figure 4a) and temperature (Figure 4c) while it increased the ice crystal effective diameter (Figure 4b). As expected, the reduction in t is most significant for the cases with thin cirrus over thick water clouds. The retrieved optical depth, for instance, decreases from 11.72 to 6.75 for Case 3, from 12.0 to 3.89 for case 6, and from 13.62 to 4.5 for case 7. The average optical depth is reduced by more than 100% for the three cases. For thick-ice-over-thin-water clouds, the estimated changes in t are around 20~40%. For example, t decreases from 11 to 7 for case 4 and 6 to 5 for Case 9. The relative change in *De* for the new algorithm is not as dramatic as that in optical depth. For Case 7, *De* increased from 71.5 to 90 μm and from 58.29 to 64.52 μm for Case 8. When the upper layer cloud becomes optically thick, say $t > 6$ or 8, the lower cloud has minimal effect on the retrieved value of *De* because a negligible amount of 3.9μm radiation from the lower cloud passes through the

upper cloud to be received by the satellite. This effect is especially evident for Cases 1-4 when the water cloud is thin. The derived ice cloud temperatures decreased from 7 to 22 K (Figure 4c) with corresponding improvements in the cloud heights (see solid lines in Figure 3).

Figure 5 shows a comparison of *IWP* derived from the MCRS with the values from the VISST and the MVI [see Equ. (1)], and from the MMCR using an algorithm that combines measurements of Doppler velocity with radar reflectivity [*Mace et al.* 2002]. The new MCRS algorithm produces smaller values than the VISST for all cases and the MVI for most cases. In all of the cases, except Case 5, the MCRS yields values of *IWP* that are closest to those from the radar retrieval. The differences are greatest for case 7 when *IWP* (in MCRS) is around 200 gm^{-2} less than the other two satellite retrievals. Both the MCRS and MVI results agree well with the MMCR data for Case 6, while the MVI is closest to the radar retrieval for Case 5. On average, for these cases, the difference between the MCRS and MMCR *IWP*s is 27 gm^{-2}, which is 37% of the mean MMCR value of 65 gm^{-2}. The difference is less than half that between the MVI and MMCR and almost 3.5 times smaller than the mean VISST-MMCR difference. Thus, it is clear for these results that the MCRS represents a marked improvement over both the MVI and the single-layer VISST retrieval. In both of the earlier algorithms, the *TWP* is the same. The MCRS reduces the *TWP*, on average, because it generates a new value of *IWP*. The improvement in *IWP* is consistent with the improvement of the cloud-top altitudes seen in Figure 3.

The accuracy of the MMCR retrieval is generally on the order of $\pm$50% and requires that the ice portion of the cloud layers is properly identified. For some of the cases in Figure 3, determining the exact boundaries of the ice cloud could result in biases in the MMCR retrieval. Validation of MCRS using the MMCR retrieval is difficult because the MMCR retrieval, in its present state, does not account for attenuation of radar energy in liquid clouds, therefore it is generally applicable only when the LWP is

relatively small and no precipitating clouds are present. Therefore, very few validation cases were found over the SGP for the period of record considered here.

5. Results and Discussion

To assess how the MCRS changes the *IWP* in the multilayered overcast cases overall, it is necessary to examine all of the results from the four sites over the 8-month period. Figure 6 compares the ice cloud properties derived using the MCRS (black bar) with the VISST (gray bar) for ice-over-water cloud systems. The major differences between the two methods are evident in the optical depth frequency distributions (Figure 6a). The optical depths derived from the MCRS are significantly shifted to smaller values. Cloudy pixels with $t < 8$ comprise more than 30% of the data compared to only 9% for the VISST retrievals. The 8-month mean optical depth drops to 29.7 from 38.6. The mean relative change in t is around 30.5% given that the relative change is defined as

$$R_c(X_{MCRS}) = \frac{(X_{VISST} - X_{MCRS})}{X_{VISST}} * 100\%, \qquad (7)$$

where X_{VISST} and X_{MCRS} are the cloud properties derived from VISST and MCRS, respectively. For *De*, the March-October mean from this study (Figure 6b) is 64.9 μm, which is 1.3 μm greater than the original VISST average *De*. The averaged relative change is ~3.79%. As expected, the ice water path (*IWP)* values derived from current algorithm (Figure 6c) are considerably smaller than those derived from VISST; the March-October mean *IWP* decreases from 844.9 gm^{-2} to 632.7 gm^{-2}. For the MCRS retrievals, clouds with *IWP* < 200 gm^{-2} account for around 40% of the total compared to only 20% of

those from VISST. The mean relative change is 33.7%, which is only slightly lager than $R_c(t)$ but much larger than that for the ice diameter.

Minnis et al. [1998] estimate ice water path from the directly derived properties as

$$IWP = t\,(a_1 D_e + a_2 D_e^2 + a_3 D_e^3), \qquad (8)$$

where a_i are regression coefficients. Using (8), it can be shown that $R_c(IWP)$ is linearly related to $R_c(t)$ and non-linearly related to $R_c(De)$. However, the dependence of $R_c(IWP)$ on $R_c(t)$ is only slightly greater than its variation with $R_c(De)$.

Figure 7 shows R_c for the three ice cloud properties as a function of VISST optical depth (t_{VISST}) for ice-over-water clouds. The t_{VISST} derived from the reflected visible radiance represents the combined effects of all cloud layers. As such, cloud overlap causes large errors in the retrievals of ice cloud optical depth, ice water path, and particle size. For more than 75% of the overcast overlapping clouds (t_{VISST} = 60, also see Figure 6a), the MCRS reduces the ice cloud optical depth and *IWP* by more than 30%. The relative change for larger optical depths is generally smaller suggesting that in those cases, the ice cloud contains most of the mass in the multilayered systems. The maximum R_c for *IWP* and t, ~ 45%, occurs at t_{VISST} =35. However, for multilayered clouds with t_{VISST} > 60, R_c for t and *IWP* decreases with the increasing of t_{VISST}. For thin overlapped clouds (t_{VISST} = 10), the results from the new algorithm indicate that *De* is underestimated by 15% (i.e., $R_c(De)$ ~ -15%), but $R_c(De)$ becomes very small when t_{VISST} exceeds 10. Given that $R_c(t)$ averages about 30% or less for t_{VISST} > 10, it is evident that the ice clouds are generally optically thick and, therefore, the initial VISST retrieval

yields a relatively accurate value of *De*. On average relative to the VISST, the MCRS reduces *t* and *IWP* by 8.9 (23%) and 212.1 gm^{-2} (25%), respectively, and increases *De* by 1.3 μm (2%).

Figure 8 compares the histogram of upper layer cloud effective temperature derived from new algorithm (solid line) and VISST (dash line). The temperatures from the new algorithms are decreased by 10 $\pm$ 12 K, on average, which translates to a height difference of ~1.4 km. The results in Figures 3 and 8 indicate that ice-cloud height derived from traditional single-layer satellite retrieval is underestimated and over classifies mid-level ice cloud coverage.

Figure 9 shows the histogram of *IWP* derived from MCRS (black bar) and MVI method (gray bar) for ice-over- water cloud systems. The major difference between the MCRS and MVI methods is that MVI method yields about 11% negative *IWP* values while there are no negative values with the new algorithm. The MVI negative *IWP* values are physically meaningless and are obtained mainly due to the uncertainties in the large *LWP* of the lower-level water clouds, the errors in the retrieved *TWP* when ice phase is assumed for whole column cloud particles, and the small signal of upper-layer thin ice cloud. Another difference between these two methods is that the MCRS yields more than 42% of the total with *IWP* = 200 gm^{-2}, while MVI method only has 28% pixels with *IWP* in the same range. The 14% difference is due to the negative *IWP* values from the MVI method. For *IWP* > 200 gm^{-2}, the frequency distribution of the current algorithm agrees well with the MVI method. Figure 10 compares the detailed histogram distribution of *IWP* for the 0-200 gm^{-2} range with bin sizes of 10 gm^{-2}. For the 0-50 gm^{-} range, the MCRS has only 2.6% of total while the MVI yields 5.3% with *IWP* value in the range of 0-50 gm^{-2}. However, the new algorithm produces more than 36.6% in the range of 51-200 gm^{-2}, while MVI method only has 22.3%. Figures 9 and 10 suggest that the MCRS can significantly improve, not only the retrieval accuracy, but also the physical meaning of the ice cloud properties in multilayered cloud

systems. The MCRS is also expected to diminish the overestimations of t and *IWP* and to increase the underestimated *De* in these same cases.

Figure 11 shows *Rc* for the ice cloud properties as functions of LWP_{MW}. For the overlapped cloud with 100 gm^{-2} < LWP_{MW} = 400 gm^{-2}, the *Rc* are very stable with values around 20% - 35% for both optical depth and *IWP*, and –3% for ice diameter. For overlapped clouds with LWP_{MW} = 100 gm^{-2}, *Rc* values are considerably smaller than for those overlapped clouds with LWP_{MW} > 100 gm^{-2} and they increase with increasing LWP_{MW}. It is not surprising because the thin water cloud should not cause a large retrieval error for VISST although the relative uncertainty for microwave techniques may be large. For overlapped cloud with LWP_{MW} > 400 gm^{-2}, *Rc* changes vary rapidly with increasing LWP_{MW}. It suggests when lower-layer water clouds are drizzling or contain large droplets, both MW techniques and the MCRS may have significant errors as a result of the precipitation-sized hydrometeors.

Figure 12 shows the sensitivity of new algorithm to the assumption of droplet size of lower layer cloud. It suggests that the retrieval properties are not sensitive to the assumed droplet size. When r_e changes from 6 μm to 8 μm (33% increase), the mean optical depth and *IWP* increase only 5.8% and 5.5%, respectively. Thus, the differences between the MCRS and radar *IWP* values in Figure 5 are not likely due to the droplet size assumption. For thin-ice-over-thin-water cloud cases, the estimated ice cloud properties may be affected by this assumption. For the lowest category of optical depth (τ < 5) in the figure, for instance, the frequency drops more than 5% when r_e changes from 8 μm to 10μm. There is almost no change for the thicker ice cloud systems.

Similarly, Figure 13 summarizes the sensitivity of the ice cloud properties to the uncertainty in *LWP* ($\pm$ 40 gm^{-2}) from the MWR retrieval. Overall, the ice cloud properties are more sensitive to an underestimate of *LWP* than to an overestimate. The optical depth increases by ~10% for 40 gm^{-2}

overestimate in *LWP* compared to only 2% for 40 gm^{-2} too much *LWP*. The Ice crystal size is only affected by $\pm$ 2%, while the uncertainty in the *LWP* translates to an uncertainty of -7.6% to 3% in *IWP*. The sensitivity is larger for smaller values of *IWP*.

6. Conclusion

A more rigorous multilayered cloud retrieval system has been developed to improve the determination of high cloud properties in multilayered clouds. The MCRS attempts a more realistic interpretation of the radiance field than earlier methods because it explicitly resolves the radiative transfer that would produce the observed radiances. A two-layer cloud model was used to simulate multilayered cloud radiative characteristics. It uses a simplified visible reflectance parameterization that could produce some uncertainties that will be examined in future studies. Surely, use of explicit two-level radiative transfer calculations could reduce the uncertainties in the retrievals. Despite the use of a simplified two-layer cloud reflectance parameterization, the MCRS clearly produced a more accurate retrieval of ice water path than the simple differencing techniques used in the past. The initial results indicate that it still might be overestimating *IWP* for overlapped cases, but by much smaller amounts than other techniques. However, many more comparisons are needed with radar-MWR retrievals and a better assessment of the errors in the radar retrievals is needed. The method is not particularly sensitive to the assumed droplet size or the uncertainties in the MWR retrievals. The errors are smaller than the differences between the radar and MCRS retrievals. Thus, this new physically based technique should be robust and directly applicable when the proper microwave and imager data are available.

Such data are available from a variety of satellites and should be exploited to derive the ice water path properties over ocean where the *LWP* can be derived reliably. Over land, the variability in surface emissivity renders the microwave approach nearly useless. Thus, surface radiometers like those at the ARM sites are the only source for applying this technique. With further validation against the radar retrievals and perhaps aircraft in situ data, the method could be used as reference source for other techniques that are available or being developed using other combinations of spectral radiances. Because it does not require the presence of cloud radar, only the microwave radiometer, this method could be applied at any location having the microwave radiometer providing the opportunities for validating other methods in many more conditions than possible using the radar retrievals. In the short term, this method will be extremely valuable for climate research by providing more accurate retrievals of ice water path than previously possible.

Acknowledgements

This research was supported by the Environmental Sciences Division of U.S. Department of Energy through the Interagency Agreements DE-AI02-97ER62341 and DE-AI02-02ER63319 under the ARM program.

References

Ackerman, T., and G. Stokes (2003), The Atmospheric Radiation Measurement Program, *Physics Today,* 56**,** 38 – 45.

Arduini, R. F., P. Minnis, and D. F. Young (2002), Investigation of a visible reflectance parameterization for determining cloud properties in multilayered clouds, *Proc. 11th AMS Conf. Cloud Physics*, Ogden, UT, June 3-7, CD-ROM, P2.4.

Benjamin, S. G., D. Devenyi, S. S. Weygandt, K. J. Brundage, J.M. Brown, G.A. Grell, D. Kim, B. E. Schwartz, T. G. Smirnova, T. L. Smith, and G. S. Manikin (2004), An hourly assimilation – forecast cycle: The RUC, Mon Wea. Rev., *132*, 495-518.

Cess, R. D., G. L. Potter, J. P. Blanchet, G. J. Boer, A. D. Del Genio, M. Deque, V. Dymnikov, V. Galin, W. L. Gates, S. J. Ghan, J. T. Kiehl, A. A. Lacis, H. Le Treut, Z.-X. Li, X.-Z. Liang, B. J. McAvaney, V. P. Meleshko, J. F. B. Mitchell, J.-J. Morcrette, D. A. Randall, L. Rikus, E. Roeckner, J. F. Royer, U. Schlese, D. A. Sheinin, A. Slingo, A. P. Sokolov, K. E. Taylor, W. M. Washington, R. T. Wetherald, I. Yagai, and M.-H. Zhang (1990), Intercomparison and interpretation of climate feedback processes in 19 atmospheric general circulation models, *J. Geophys, Res., 95***,** 16601-16615.

Clothiaux, E. E., T. P. Ackerman, G. G. Mace, K. P. Moran, R. T. Marchand, M. Miller, and B. E. Martner (2000), Objective determination of cloud heights and radar reflectivities using a combination of active remote sensors at the ARM CART sites, *J. Appl. Meteorol., 39*, 645-665.

Ho, S.-P., B. Lin, P. Minnis, and T.-F. Fan (2003), Estimation of cloud vertical structure and water amount over tropical oceans using VIRS and TMI data, *J. Geophys. Res., 108*, 10.1029/2002JD003298.

Huang, J. P., M. M. Khaiyer, P. W. Heck, P. Minnis, and B. Lin (2003), Determination of ice-water path over the ARM SGP using combined surface and satellite datasets. *Proc. 13th ARM Science Team Meeting*, Broomfield, CO, March 31 - April 4, 2003.

Liljegren, J.C. (1999), Automatic self-calibration of ARM microwave radiometers. *Microwave Radiometry and Remote Sensing of the Earth's Surface and Atmosphere*, Eds. P. Pampaloni and S. Paloscia, pp. 433-443, VSP Press.

Lin, B., and W. B. Rossow (1996), Seasonal variation of liquid and ice water path in non-precipitating clouds over oceans, *J. Climate*, *9,* 2890-2902.

Lin, B., P. Minnis, B. Wielicki, D. R. Doelling, R. Palikonda, D. F. Young, and T. Uttal (1998), Estimation of water cloud properties from satellite microwave, infrared and visible measurements in oceanic environments, II: Results. *J. Geophys, Res.*, *103,* 3887-3905.

Lin, B., P. Minnis, A. Fan, J. A. Curry, and H. Gerber (2001), Comparison of cloud liquid water paths derived from in situ and microwave radiometer data taken during the SHEBA/FIREACE, *Geophys. Res. Lett*., *28*, 975-978.

Liu, G., and J. A. Curry (1998), Remote sensing of ice water characteristics in tropical clouds using aircraft microwave data, *J. Appl. Meteorol.*, *37*, 337-355.

Liu, G., and J. A. Curry (1999), Tropical ice water amount and its relations to other atmospheric hydrological parameters as inferred from satellite data, *J. Appl. Meteorol.*, *38*, 1182-1194.

Mace, G. G., A. J. Heymsfield, and M. R. Poellot (2002), On retrieving the microphysical properties of cirrus clouds using the moments of the millimeter-wavelength Doppler spectrum, *J. Geophys. Res.*, *107*, 4815-4841.

Mace, G. G., Y. Zhang, S. Platnick, M. D. King, P. Minnis, and P. Yang (2004), Evaluation of cirrus cloud properties from MODIS radiances using cloud properties derived from ground-based data collected at the ARM SGP site. Accepted, *J. Appl. Meteorol.*.

Minnis, P., Y. Takano, and K.-N. Liou (1993), Inference of cirrus cloud properties using satellite-observed visible and infrared radiances, Part I: Parameterization of radiance fields, *J. Atmos. Sci.*, 50, 1279-1304.

Minnis, P., D. F. Young, D. P. Kratz, J. A. Coakley, Jr., M. D. King, D. P. Garber, P. W. Heck, S. Mayor, and R. F. Arduini, Cloud Optical Property Retrieval (Subsystem 4.3) (1995). "Clouds and the Earth's Radiant Energy System (CERES) Algorithm Theoretical Basis Document, Volume III: Cloud Optical Property Retrieval (Subsystem 4.3)", *NASA RP 1376 Vol. III*, edited by CERES Science Team, pp. 135-176.

Minnis, P., D. P. Garber, D. F. Young, R. F. Arduini, and Y. Takano (1998), Parameterization of reflectance and effective emittance for satellite remote sensing of cloud properties, *J. Atmos. Sci.*, 55, 3313-3339.

Minnis, P., W. L. Smith, Jr., D. F. Young, L. Nguyen, A. D. Rapp, P. W. Heck, S. Sun-Mack, Q. Trepte, and Y. Chen (2001), A near-real time method for deriving cloud and radiation properties from satellites for weather and climate studies, *Proc. AMS 11th Conf. Satellite Meteorology and Oceanography*, Madison, WI, Oct. 15-18, 477-480.

Minnis, P., L. Nguyen, D. R. Doelling, D. F. Young, W. F. Miller, and D. P. Kratz(2002), Rapid calibration of operational and research meteorological satellite imagers, Part I: Evaluation of research satellite visible channels as references, *J. Atmos. Oceanic Technol.*, *19*, 1233-1249.

Weng, F, and N. C. Grody (2000), Retrieval of ice cloud parameters using a microwave imaging radiometer, *J. Atmos. Sci., 57*, 1069-1081.

Zhao, L. and F. Weng (2002), Retrieval of ice cloud parameters using the advanced microwave sounding unit, *J. Appl. Meteorol., 41***,** 384-395.

Figure Captions

Figure 1 Reflectance at 0.65μm as a function of total cloud water path from adding-doubling RTM calculations for 6 sets of viewing and illumination conditions. The solid curves are for a single-layer ice cloud (T40 model with *De* = 67 μm) and the broken curves are for a T40 ice cloud over a water cloud with LWP = 100 gm^{-2}. Results are shown for *re* = 8 and 12 μm. In each panel, the thick solid and broken curves represent results with smaller viewing angle (30^o), and the thin ones are for larger viewing angle (60^o).

Figure 2 Schematic view of the multilayered cloud retrieval system (MCRS).

Figure 3 Millimeter Wave Cloud Radar (MMCR) reflectivity observed at ARM SGP central facility site for ten multilayered cloud cases. The solid red and dashed lines represent the cloud height derived from MCRS and VISST, respectively.

Figure 4 Comparison of ice cloud properties derived from MCRS and VISST for the 10 cases shown in Fig. 3.

Figure 5 Comparison of ice water path (IWP) derived from the MCRS, VISST, MVI differencing (TWP - LWP), and Millimeter Wave Cloud Radar (MMCR) reflectivity for the 10 cases shown in Fig. 3.

Figure 6 Comparison of ice cloud properties derived from MCRS (black bar) with VISST (gray bar) for (a) optical depth, (b) ice diameter, and (c) ice water path for ice-over-water clouds over four ARM SGP sites (March-October, 2000). The histogram bins are 5 for (a), 5 μm for (b), and 200 gm^{-2} for (c).

Figure 7 Relative change rates of ice cloud properties derived from MCRS to the properties derived from VISST as a function of VISST optical depth for ice-over-water clouds over four ARM SGP sites (March-October, 2000). Solid line is for IWP, dot line for optical depth and dash line for ice diameter.

Figure 8 Comparison of cloud effective temperature derived from MCRS (solid line) and VISST (dished line) for ice-over-water cloud systems over four ARM SGP sites (March-October, 2000). The histogram bin is 5 K.

Figure 9 Comparison of ice water path derived from MCRS (black bar) and MVI (gray bar) for ice-over-water cloud systems over four ARM SGP sites (March-October, 2000). The histogram bin is 200 gm^{-2}. The 0-200 gm^{-2} range bin is represented by 0.

Figure 10 Detailed view of the 0-200 gm^{-2} histogram bin shown in Fig.9 using 10 gm^{-2} bins.

Figure 11 Same as Fig.7 but as a function of microwave LWP of lower level water cloud.

Figure 12 Comparison of MCRS sensitivity to lower layer water cloud droplet size assumption for ice-over-water cloud over four ARM SGP sites (March-October, 2000): Re= 6 μm (black bar), 8 μm (gray bar), and 10μm (light gray bar).

Figure 13 Comparison of MCRS Sensitivity to error in microwave LWP for ice-over-water cloud over four ARM SGP sites (March-October, 2000): LWP (+40 gm^{-2}) (black bar), LWP (+0 gm^{-2}) (gray bar), and LWP (-40 gm^{-2}) (light gray bar).

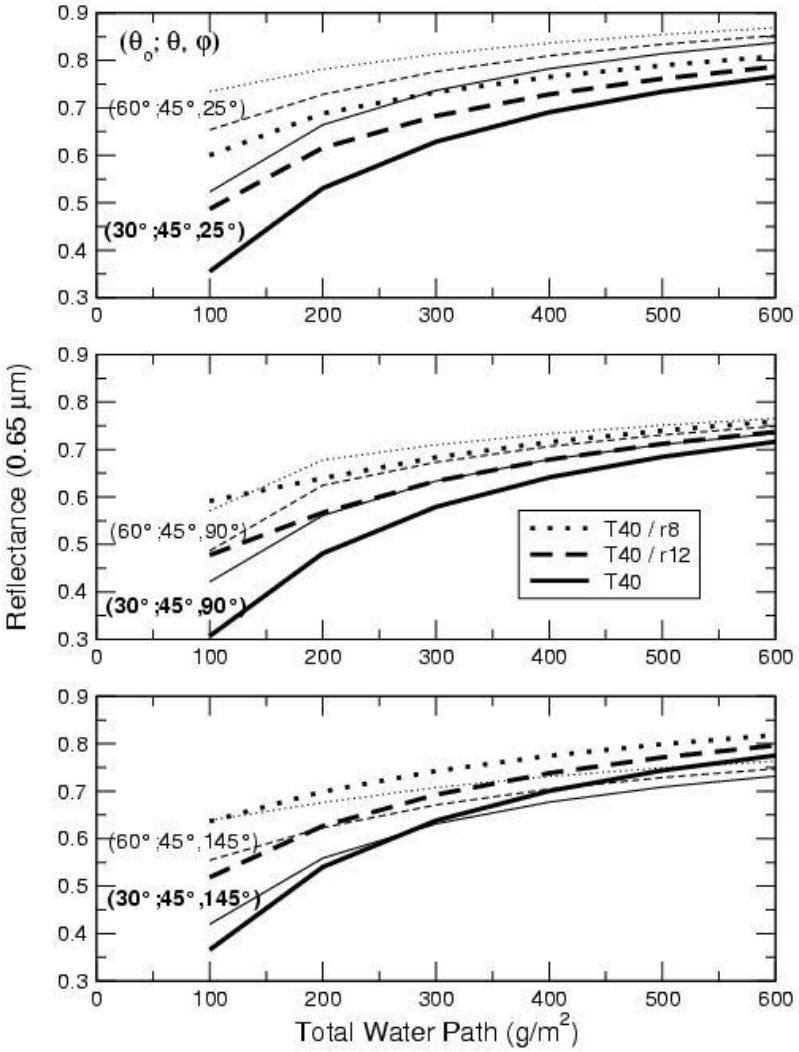

Figure 1 Reflectance at 0.65 µm as a function of total cloud water path from adding-doubling RTM calculations for 6 sets of viewing and illumination conditions. The solid curves are for a single-layer ice cloud (T40 model with *De* = 67 µm) and the broken curves are for a T40 ice cloud over a water cloud with LWP = 100 gm^{-2}. Results are shown for *re* = 8 and 12 µm. In each panel, the thick solid and broken curves represent results with smaller viewing angle (30^o), and the thin ones are for larger viewing angle (60^o).

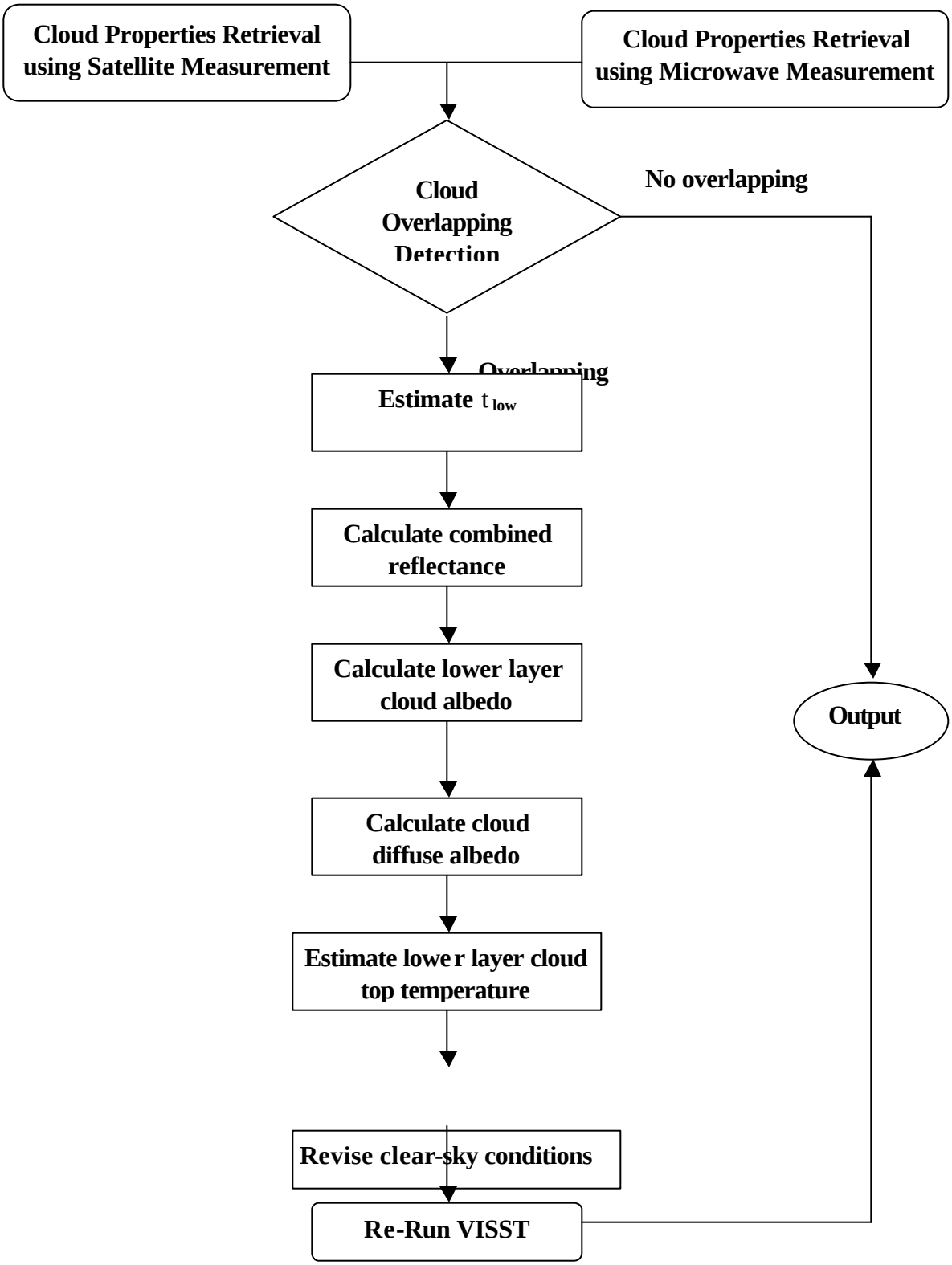
Cloud Properties Retrieval using Satellite Measurement
Cloud Properties Retrieval using Microwave Measurement
Cloud Overlapping Detection
No overlapping
Overlapping
Estimate t_{low}
Calculate combined reflectance
Calculate lower layer cloud albedo
Calculate cloud diffuse albedo
Estimate lower layer cloud top temperature
Revise clear-sky conditions
Re-Run VISST
Output

Figure 2 Schematic view of the multilayered cloud retrieval system (MCRS).

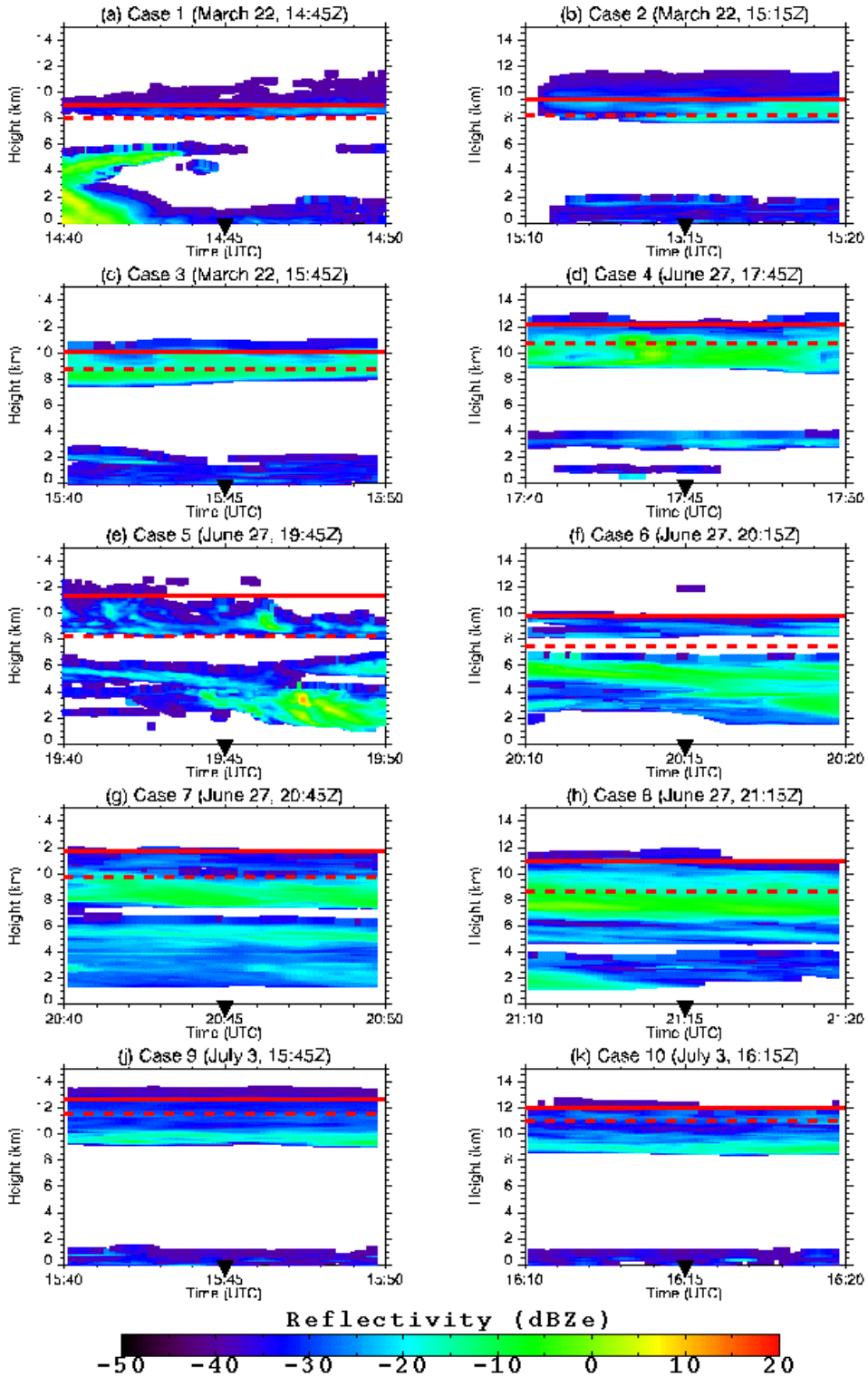
(a) Case 1 (March 22, 14:45Z)
(b) Case 2 (March 22, 15:15Z)
(c) Case 3 (March 22, 15:45Z)
(d) Case 4 (June 27, 17:45Z)
(e) Case 5 (June 27, 19:45Z)
(f) Case 6 (June 27, 20:15Z)
(g) Case 7 (June 27, 20:45Z)
(h) Case 8 (June 27, 21:15Z)
(j) Case 9 (July 3, 15:45Z)
(k) Case 10 (July 3, 16:15Z)
Height (km)
Time (UTC)
Reflectivity (dBZe)
-50 -40 -30 -20 -10 0 10 20

Figure 3 Millimeter Wave Cloud Radar (MMCR) reflectivity observed at ARM SGP central facility site for ten multilayered cloud cases. The solid red and dashed lines represent the cloud height derived from MCRS and VISST, respectively.

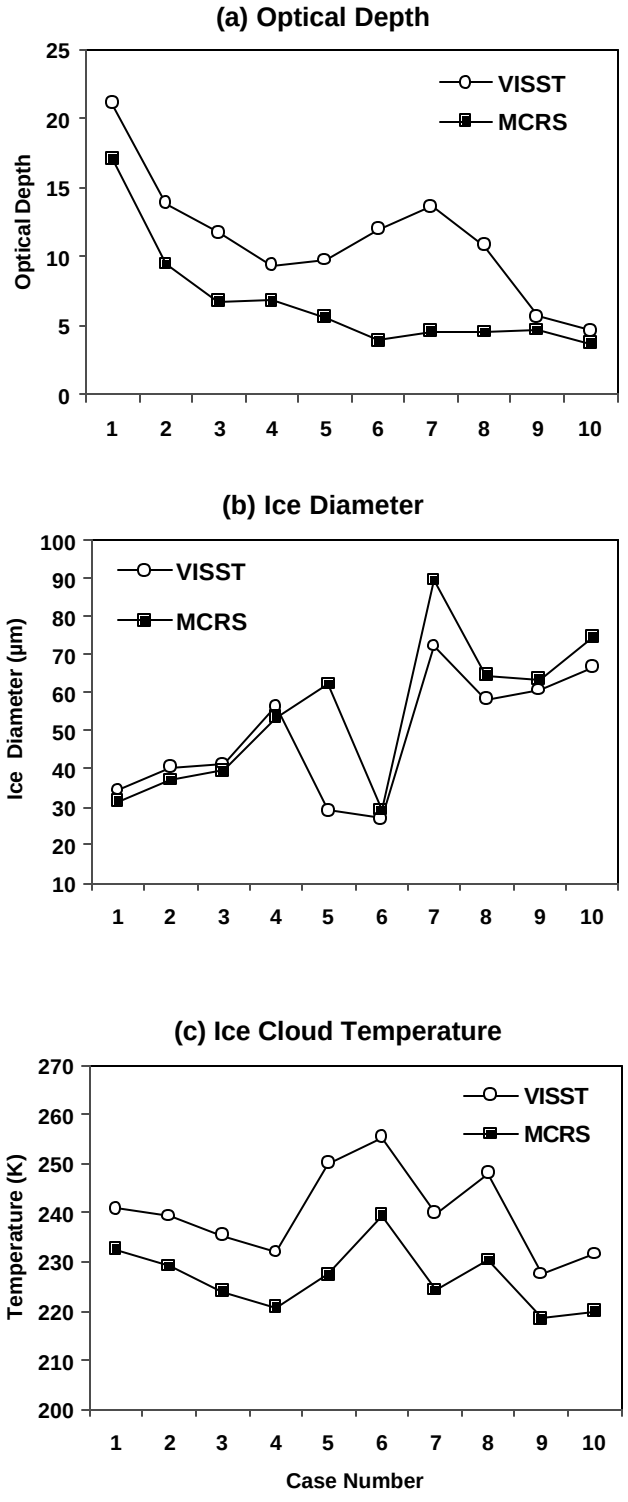

Figure 4 Comparison of ice cloud properties derived from MCRS and VISST for the 10 cases shown in Fig. 3.

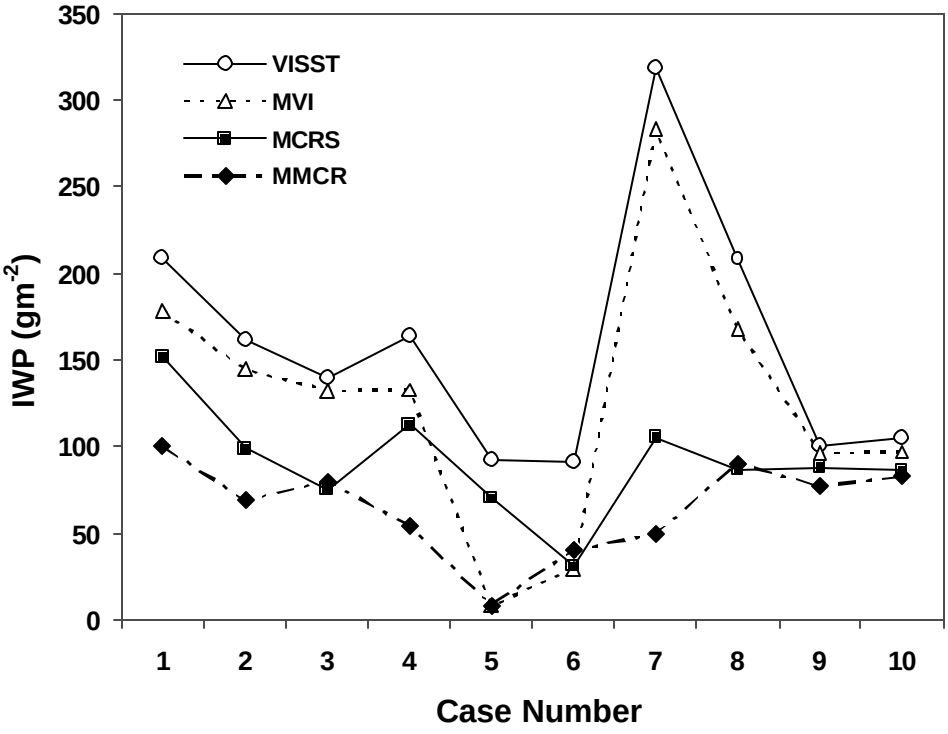

Figure 5 Comparison of ice water path (IWP) derived from the MCRS, VISST, MVI differencing (TWP - LWP), and Millimeter Wave Cloud Radar (MMCR) reflectivity for the 10 cases shown in Fig. 3.

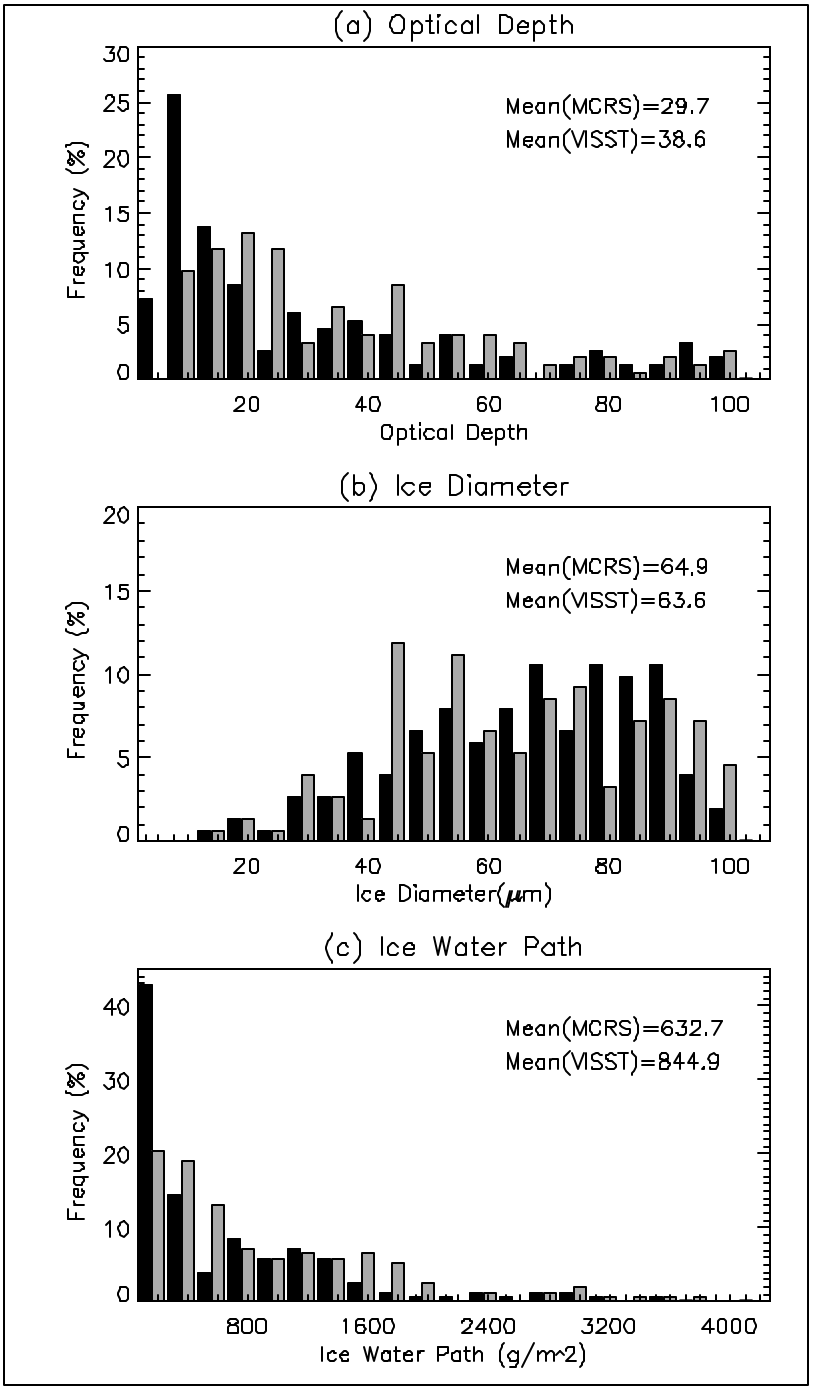

Figure 6 Comparison of ice cloud properties derived from MCRS (black bar) with VISST (gray bar) for (a) optical depth, (b) ice diameter, and (c) ice water path for ice-over-water clouds over four ARM SGP sites (March-October, 2000). The histogram bins are 5 for (a) and 5μm for (b), and 200 gm^{-2} for (c).

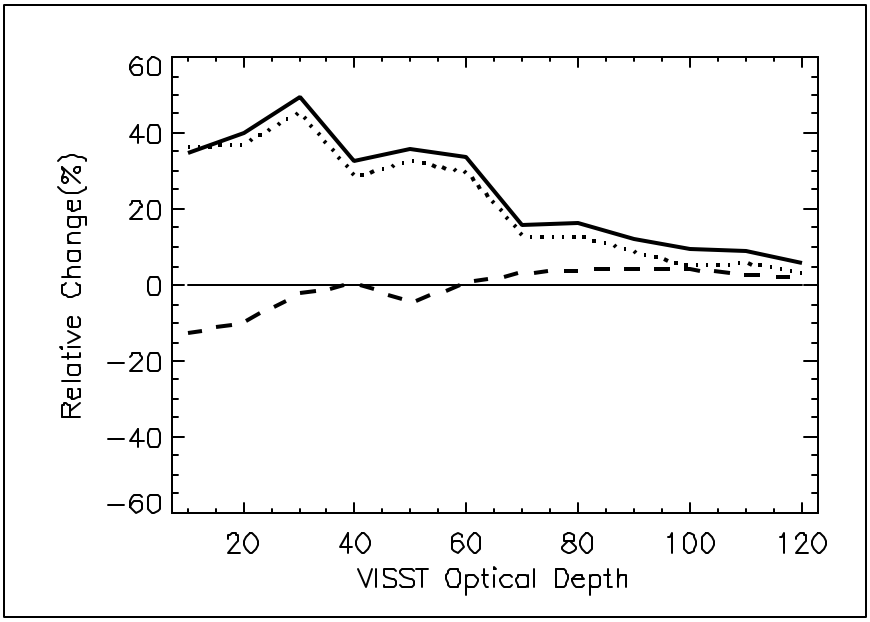

Figure 7 Relative change rates of ice cloud properties derived from MCRS to the properties derived from VISST as a function of VISST optical depth for ice-over-water clouds over four ARM SGP sites (March-October, 2000). Solid line is for IWP, dot line for optical depth and dash line for ice diameter.

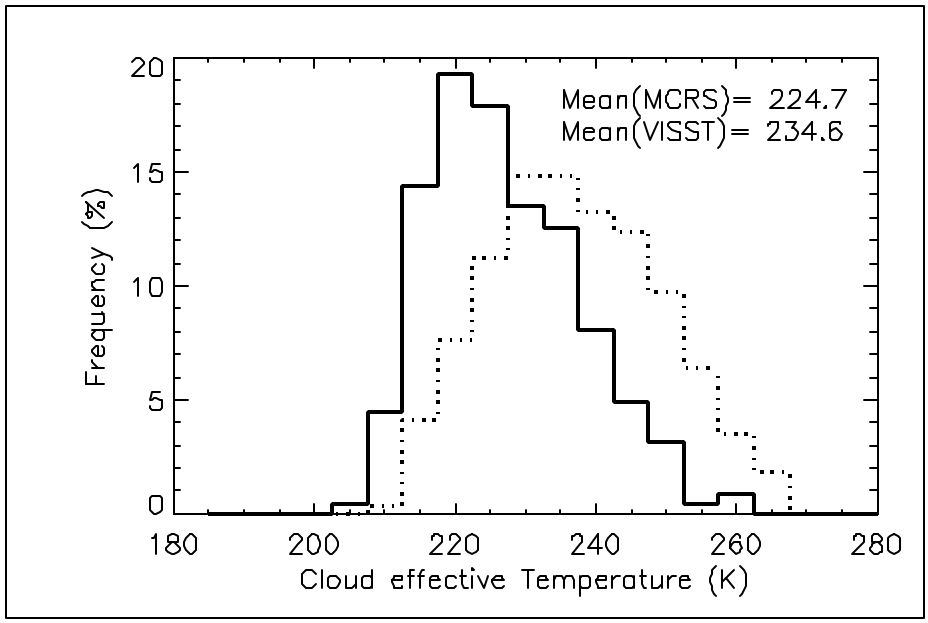

Figure 8 Comparison of cloud effective temperature derived from MCRS (solid line) and VISST (dished line) for ice-over-water cloud systems over four ARM SGP sites (March-October, 2000). The histogram bin is 5 K.

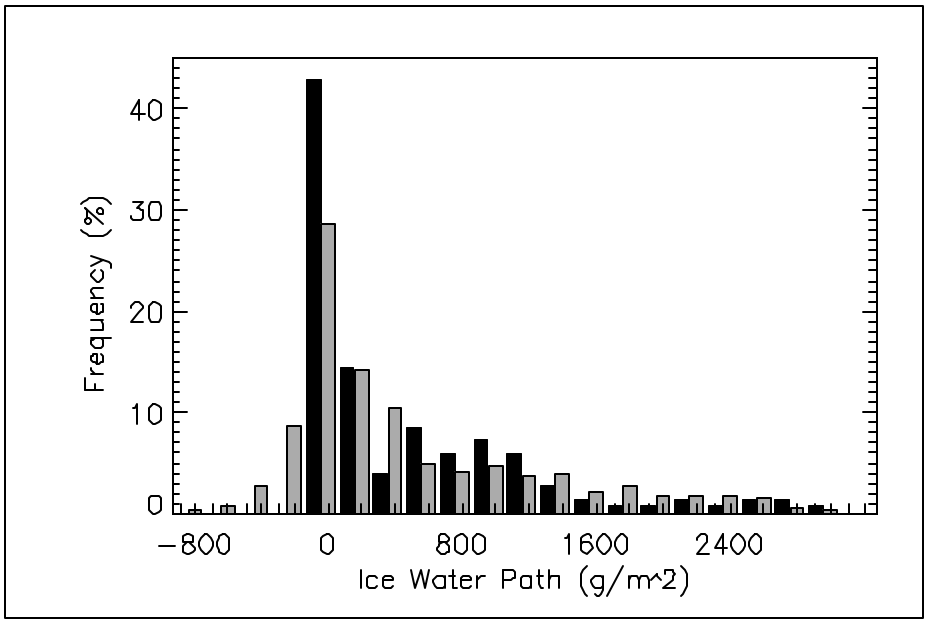

Figure 9 Comparison of ice water path derived from MCRS (black bar) and MVI (gray bar) for ice-over-water cloud systems over four ARM SGP sites (March-October, 2000). The histogram bin is 200 gm^{-2}. The 0-200 gm^{-2} range bin is represented by 0.

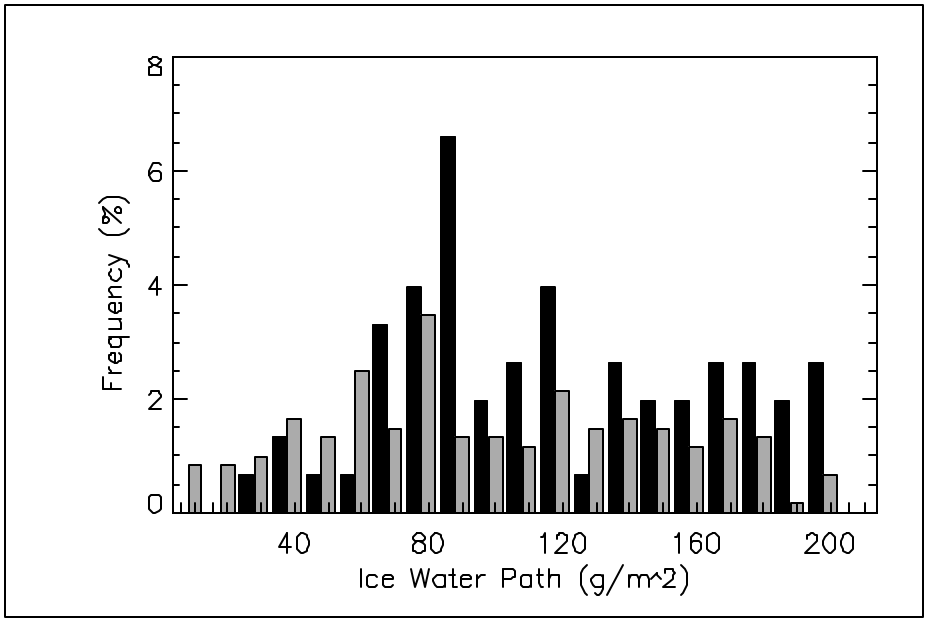

Figure 10 Detailed view of the 0-200 gm^{-2} histogram bin shown in Fig.9 using 10 gm^{-2} bins.

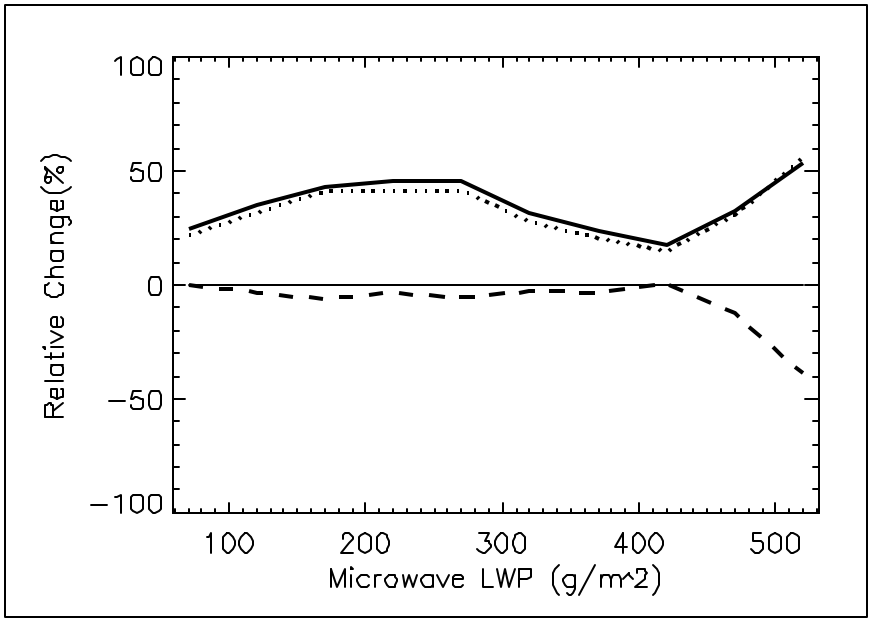

Figure 11 Same as Fig.7 but as a function of microwave LWP of lower level water cloud.

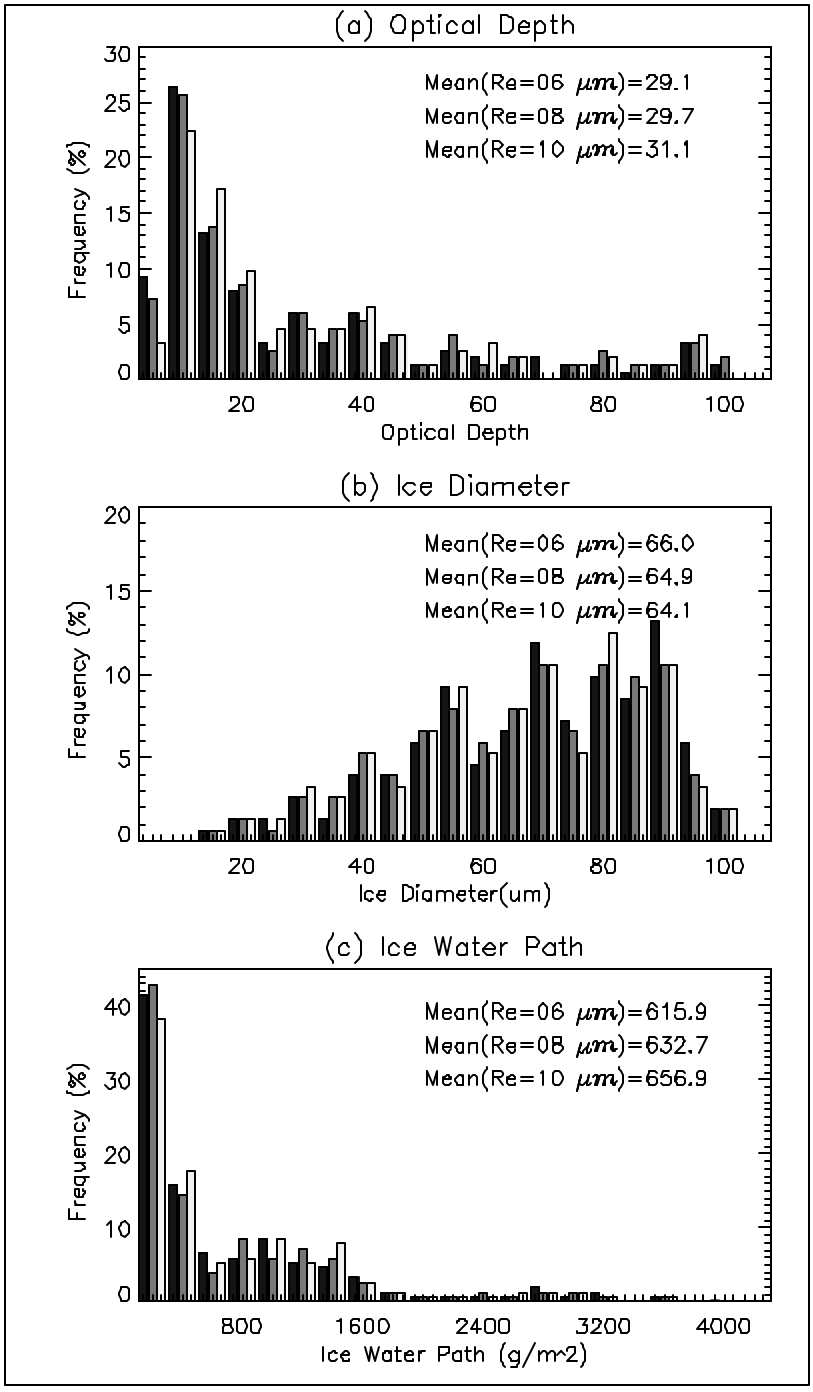

Figure12 Comparison of MCRS sensitivity to lower layer water cloud droplet size assumption for ice-over-water cloud over four ARM SGP sites (March-October, 2000): Re = 6 μm (black bar), 8 μm (gray bar), and 10 μm (light gray bar).

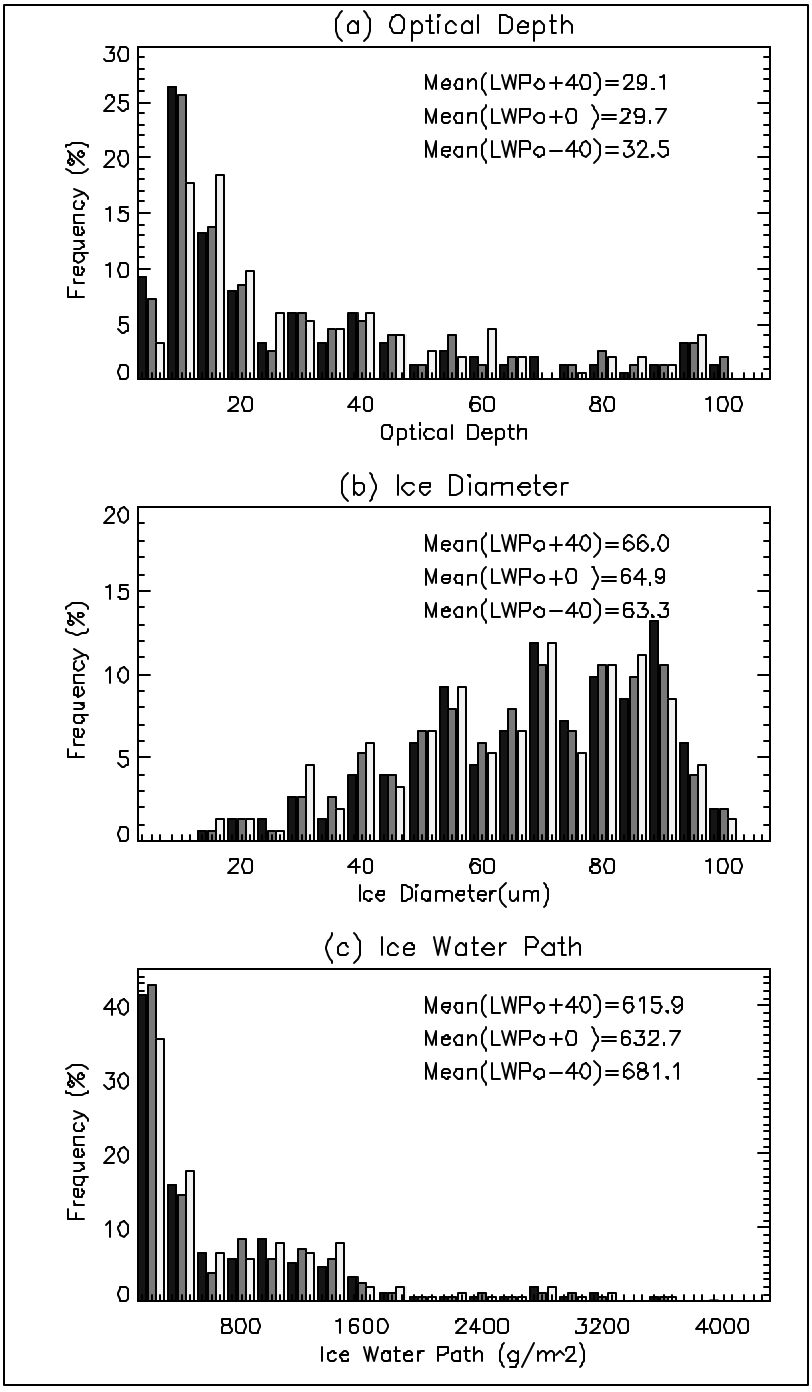

Figure 13 Comparison of MCRS Sensitivity to error in microwave LWP for ice-over-water cloud over four ARM SGP sites (March-October, 2000): LWP (+40 gm^{-2}) (black bar), LWP (+0 gm^{-2}) (gray bar), and LWP (-40 gm^{-2}) (light gray bar).